RESEARCH ARTICLE

An experimental study on a suction flow control method to reduce the unsteadiness of the wind loads acting on a circular cylinder

Wen-Li Chen · Hui Li · Hui Hu

Abstract An experimental investigation was conducted to assess the effectiveness of a suction flow control method for vortex-induced vibration (VIV) suppression. The flow control method uses a limited number of isolated suction holes to manipulate the vortex shedding in the wake behind a circular cylinder in order to reduce the unsteadiness of the dynamic wind loads acting on the cylinder. The experimental study was performed at $Re \approx 3.0 \times 10^4$, i.e., in the typical Reynolds number range of VIV for the cables of cable-stayed bridges. In addition to measuring the surface pressure distributions to determine the resultant dynamic wind loads acting on the test model, a digital particle image velocimetry system was used to conduct detailed flow field measurements to reveal the changes in the shedding process of the unsteady wake vortex structures from the test model with and without the suction flow control. The effects of important controlling parameters (i.e., the azimuthal locations of the suction holes in respect to the oncoming airflow, the spanwise spacing between the suction holes, and the suction flow rate through the suction holes) on the wake flow characteristics, the surface pressure distributions, and the resultant dynamic wind loads were assessed quantitatively. While a higher suction flow rate and smaller spanwise spacing between the suction holes were beneficial to the effectiveness of the suction flow control, the azimuthal locations of the suction holes were found to be very critical for reducing the fluctuating amplitudes of the dynamic wind loads acting on the test model using the suction flow control method. With the suction holes located at the proper azimuthal locations on the test model (i.e., at the azimuthal angle of $\theta = 90°$ and $270°$ for the present study), the characteristics of the wake flow behind the test model were found to change significantly along the entire span of the test model, even though only a limited number of the isolated suction holes were used for the suction flow control. The detailed flow field measurements were correlated with the measured surface pressure distributions and the resultant dynamic wind loads acting on the test model to gain further insight into the fundamental mechanism of the suction flow control method for VIV suppression.

W.-L. Chen · H. Hu (✉)
Department of Aerospace Engineering, Iowa State University, Ames, IA 50011, USA
e-mail: huhui@iastate.edu

W.-L. Chen · H. Li
Key Lab of structures Dynamic Behavior and Control (Harbin Institute of Technology), Ministry of Education, Harbin 150090, Heilongjiang, People's Republic of China

W.-L. Chen · H. Li
School of Civil Engineering, Harbin Institute of Technology, Harbin 150090, Heilongjiang, People's Republic of China

1 Introduction

Inclined circular cables are the key components of cable-stayed bridges. Inclined circular cables often vibrate under windy and/or rainy conditions, which are usually referred as vortex-induced vibration (VIV) (Main and Jones 1999; Matsumoto et al. 2003; Zuo et al. 2008; Zuo and Jones 2010; Hikami and Shiraishi 1988; Li et al. 2010; Chen et al. 2011, 2013a). As reported by Zuo et al. (2008) in a field study of the VIVs of the stay cables on Fred Hartman Bridge in Houston, TX, USA, VIV of a circular cable is a self-limiting vibration, which occurs quite frequently at lower wind speeds. It has been suggested that frequent VIVs of cables may induce fatigue damage to the cables. Therefore, it is highly desirable to reduce the VIVs of

cables to improve their fatigue lifetime, thereby, improving the durability of the cable-stayed bridges.

Since VIV phenomena are closely related to the unsteady vortex shedding in the wakes behind bluff bodies (i.e., circular cylinders), a number of studies have been performed in recent years to manipulate the vortex shedding process to reduce the VIVs. Several passive flow control methods, which depend on the modifications of the geometry of the bluff bodies, have been suggested to manipulate the vortex shedding process in the wakes behind the bluff bodies. For example, Roshko (1955, 1961) suggested mounting a splitter plate behind a circular cylinder to change the alternating shedding mode of the vortex structures in the wake flow into a symmetric shedding mode. Owen and Bearman (2001) attached hemispherical bumps to circular cylinders to control the fluctuating amplitudes of the vortex-induced vibrations of cable models.

A number of active flow control methods have also been suggested to control the vortex shedding in the wakes behind bluff bodies to suppress VIVs. For examples, Wu et al. (2007) suggested using a moving wall (i.e., generating an appropriate transverse wave propagating along the surface of a circular cylinder) to control the flow separation over a circular cylinder. Their numerical simulation results showed that this active flow control method would allow the oncoming flow streams to remain attached on the entire surfaces of the cylinder and eliminate the shedding of unsteady vortices in the wake flow. Modi (1997), Munshi et al. (1997) and Patnaik and Wei (2002) used a momentum injection method to control the flow separation around airfoils, flat plates, rectangular prisms, D-section prisms, and circular cylinders, and found that the momentum injection method could effectively suppress the VIV and galloping instabilities by controlling the flow separation. Grager et al. (2011) used a dynamic burst control plate to suppress airfoil stalls by preventing the separation bubble from bursting near the leading edge of a low Reynolds number airfoil. Synthetic jets (i.e., zero-net mass flux) have also been suggested to control/suppress flow separation and vortex shedding from various bluff bodies. Glezer and Amitay (2002) investigated the interactions of synthetic jets with cross-flows and reported that synthetic jets could delay flow separation and reduce the drag acting on bluff bodies. While synthetic jets were usually placed near the separation points for flow control, Feng et al. (2010, 2011) and Feng and Wang (2010, 2012) found that synthetic jets located at the rear stagnation points of circular cylinders could also be used to suppress flow separation and reduce the drag acting on the circular cylinders.

Suction flow control methods have also been suggested to suppress flow separation over airfoils (Qin et al. 1998;

Greenblatt et al. 2006; Gbadebo et al. 2008; Chng et al. 2009), plates (Seal and Smith 1999; Fransson and Alfredsson 2003) and circular cylinders (Fransson et al. 2004; Patil and Ng 2010). Patil and Ng (2010) used a spanwise periodic porosity on the surface of a circular cylinder with suction flow control to suppress flow separation. They found that the periodic porosity with suction flow control would induce a series of steady counter-rotating vortex structures behind the porous patches, which would lead to a reduction in drag, a suppression of the formation of the spanwise vortices, and a reduction in the fluctuating amplitudes of the aerodynamic forces acting on the circular cylinder. Fransson et al. (2004) studied the flow field around a porous circular cylinder with flow suction pores distributed on its surface. They found that a moderate level of flow suction control would have a large impact on the flow field around the circular cylinder; namely the suction flow control could delay flow separation, resulting in a much narrower wake and the drag reduction. More recently, Chen et al. (2013b) reported an experimental study to investigate the effectiveness of a suction control method using a limited number of isolated suction holes to suppress VIV of a cylindrical cable model. They found that, even though only a limited number of suction holes were used for the suction flow control, the VIV of the cylindrical cable model was suppressed greatly under the suction flow control condition. The measurement results reported in Chen et al. (2013b) reveal many interesting features of the VIV phenomena with and without suction flow control; however, because the main objectives of Chen et al. (2013b) were focused on quantifying the global characteristics of the VIV phenomena by measuring the vibration responses of a spring–mass system, the characteristics of the corresponding flow fields around the test model with and without suction flow control were not investigated in that study. Quantitative information of the flow fields around the test model with and without suction flow control is highly desirable for developing a better understanding of the fundamental mechanism of the suction control method.

The work reported in the present study can be considered as a follow-on study of the work reported in Chen et al. (2013b), which was conducted to further assess the effectiveness of the suction flow control method in reducing the fluctuating amplitudes of the dynamic wind loads (i.e., both the lift and drag forces) acting on the test model for VIV suppression. The experimental study was performed at $Re \approx 3.0 \times 10^4$, i.e., in the range of the Reynolds numbers of VIV for the circular cables of cable-stayed bridges. In addition to measuring the instantaneous surface pressure distributions to determine the resultant dynamic wind loads (i.e., the time-averaged values and the fluctuating amplitudes of the aerodynamic forces) acting on

the test model, a digital particle image velocimetry (PIV) system was used to conduct detailed flow field measurements to quantify the shedding process of unsteady vortex structures in the wake behind the test model with and without suction flow control. The effects of important controlling parameters—such as the azimuthal locations of the isolated suction holes in relation to the oncoming flow, the spanwise spacing between the isolated suction holes, and the suction flow rate through the suction holes, on the wake flow characteristics, the surface pressure distributions around the test model, and the resultant dynamic wind loads acting on the test model—were assessed quantitatively. The detailed flow field measurements were correlated with the measured surface pressure distributions and the resultant dynamic aerodynamic forces acting on the test model to elucidate the underlying physics and to explore/optimize design paradigms for the development of innovative and robust flow control approaches for VIV suppression.

2 Test model and experimental setup

2.1 The cylindrical test model used in the present study

The experimental study was conducted in a low-speed, closed-loop wind tunnel located in the Aerospace Engineering Department of Iowa State University. The tunnel has a test section of 1.0 × 1.0 ft (0.305 m × 0.305 m) in cross section with optically transparent walls. The wind tunnel has a contraction section upstream of the test section with a set of honeycombs, screen structures, and a cooling system installed ahead of the contraction section to provide uniform low turbulent airflow into the test section. The turbulence intensity level in the test section of the wind tunnel was about 0.8 %, measured by using a hotwire anemometer.

It should be noted that, while the yaw angle of the oncoming airflow and the inclined angle of a stay cable would affect the VIV characteristics of the stay cable, by using the inclined cable as the reference frame, the oncoming airflow can always be decomposed into a cross-flow component (i.e., the component orthogonal to the cable) and an axial flow component (i.e., the component parallel to the axis of the cable). Since the axial flow component is along the axis of the inclined cable, it does not result in the shedding of unsteady vortex structures from the cable in general. The cross-flow component, which is orthogonal to the cable, is believed to be the main reason to cause the periodic shedding of unsteady vortex structures from the cable to excite VIV. Therefore, it is a common practice in studies of the VIV phenomena of stay cables to simplify the complex 3-D problem of an inclined
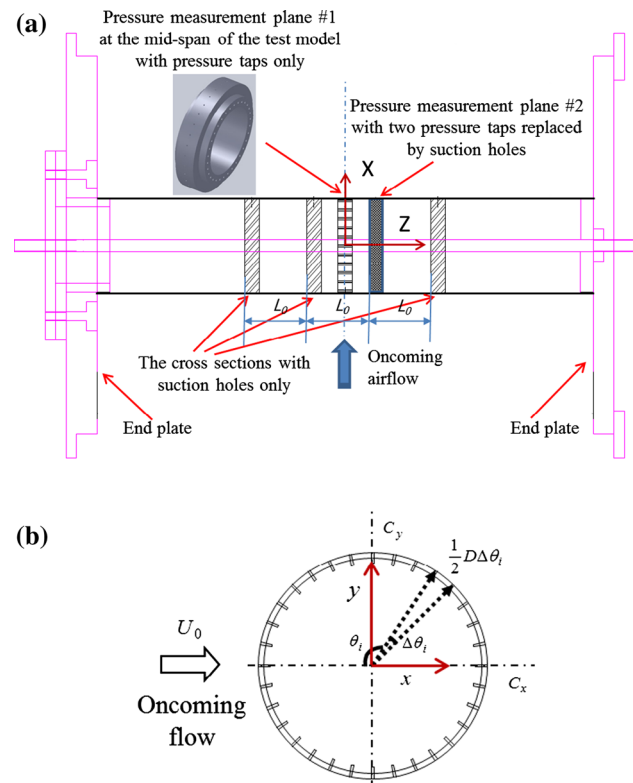

Fig. 1 The cylindrical test model used in the present study. **a** Top view of the test model. **b** The cross section of the test model with pressure taps

cable with a yaw angle to the oncoming airflow by using a 2-D cylindrical model placed in an airflow orthogonal to the test model (i.e., only consider the cross-flow component).

Figure 1 shows the schematic of the 2-D cylindrical model used in the present study. The cylindrical model, which has a diameter of 2.0 inches (i.e., $D = 0.0508$ m) and spanwise length of 12.0 inches (i.e., $L = 0.305$ m, which is equal to the width of the wind tunnel test section), was mounted horizontally in the wind tunnel test section. During the experiments, the wind speed of the oncoming airflow in the test section was fixed at 8.0 m/s (i.e., $U_\infty = 8.0$ m/s), and the corresponding Reynolds number, based on the diameter of the test model and the oncoming flow velocity, was about $Re \approx 3.0 \times 10^4$. It should be noted that, Chen et al. (2011) and Zuo et al. (2008) observed VIVs of stayed cables in field experiments at the Reynolds number levels of $Re \approx 3.3 \times 10^4$ and 3.5×10^4, respectively, which are on the same order of the Reynolds number used in the present study.

Unlike the test model used by Chen et al. (2013b), with only one set of isolated suction holes aligned evenly along the spanwise direction of the test model at the azimuthal

angle of $\theta = 270°$ in respect to the oncoming airflow, the test model used in the present study has two sets of suction holes (i.e., two suction holes at each cross-plane) with the same diameter of 3.0 mm located symmetrically on the test model in respect to the oncoming flow. During the experiments, the azimuthal locations of the suction holes were selected from $\theta = 67.5°$ and $292.5°$ (i.e., on the front face of the test model), $\theta = 90°$ and $270°$, and $\theta = 112.5°$ and $247.5°$ (i.e., on the leeward side of the test model) to assess the effectiveness of suction flow control at different azimuthal locations for VIV suppression; specifically, to assess how azimuthal location of the suction holes affects the wake vortex shedding and the unsteadiness of the dynamic wind loads acting on the test model. The spanwise spacing between the suction holes, L_0, was varied from $L/8$ to $L/4$, to investigate the effects of the spanwise spacing of the suction holes on the effectiveness of the suction flow control.

In the present study, a mass flow controller (Omega® FMA-2613A) was used to control the suction flow rate thorough the suction holes. The experiments were performed at four suction flow rates, $Q = 20, 40, 60,$ and 80 l/min, with corresponding flow velocity in each suction hole, $\bar{U}_{suc} = 5.89, 11.79, 17.68,$ and 23.58 m/s, respectively. It should be noted that the suction flow rate has been corrected to standard conditions (i.e., at the ambient temperature of 25 °C and one standard atmosphere pressure of 101.325 kPa). Following the work of Chen et al. (2013b), the suction momentum coefficient, C_μ (defined as the ratio of the suction momentum flux to the oncoming free-stream momentum flux, $C_\mu = 2\left(\frac{\bar{U}_{suc}}{U_\infty}\right)^2\left(\frac{S_{suc}}{DL_0}\right)$), was calculated. Here, S_{suc} is the area of the suction holes at each suction section (i.e., the total area of the two suction holes), and L_0 is the spacing between two neighboring suction sections. The suction flow rate and the corresponding suction momentum coefficients C_μ for each test case are listed in Table 1.

Table 1 The suction flow rate and corresponding suction momentum coefficients of the test cases in the present study

Test cases	#1	#2	#3	#4	#5
Suction flow rate (l/min)	0	20	40	60	80
Suction flow velocity (m/s)	0	5.89	11.79	17.68	23.58
Suction momentum coefficients with spanwise spacing $L_0 = L/8$	0	0.0040	0.0159	0.0357	0.0635
Suction momentum coefficients with spanwise spacing $L_0 = L/4$	0	0.0079	0.0317	0.0713	0.127

2.2 Experimental setup for surface pressure distribution measurements

In the present study, 62 pressure taps were arranged in two cross sections for the surface pressure measurements around the test model. As shown in Fig. 1b, while 32 pressure taps were evenly distributed in the cross section at the mid-span of the test model (i.e., the pressure measurement plane #1), the rest of the 30 pressure taps were distributed in one of the cross sections with suction holes (i.e., the pressure measurement plane #2 shown in Fig. 1a) with two of the pressure taps replaced by the two suction holes. The pressure taps were connected to four units of digital sensor arrays (DSA3217, Scanivalve Corp®, 16 channels for each unit) by using tygon tubing with 1.5 mm diameter and 0.5 m length for the pressure data acquisition. The DSA3217 system incorporates temperature-compensated piezo-resistive pressure sensors with a pneumatic calibration valve, RAM, 16 bit A/D converter, and a microprocessor in a compact self-contained module. The precision of the pressure acquisition system is ±0.05 % of the ±10 inch H_2O full scale range. During the experiments, the instantaneous surface pressure measurement data for each pressure tap were acquired for 100 s at a data acquisition rate of 300 Hz. Based on the work of Irwin et al. (1979), the amplitude attenuation and phase lag of the instantaneous pressure signals caused by the 1.5-mm-diameter, 0.5-m-long tygon tubing used for the surface pressure measurements are expected to be quite small for the test cases of the present study (i.e., at a data acquisition frequency less than 300 Hz). The solid blockage and the wake blockage effects of the test model on the pressure measurements were corrected, as suggested by Barlow et al. (1999).

Based on the integration of the measured surface pressure distributions around the test model, the resultant wind loads (i.e., the lift and drag forces) acting on the test model can be determined by neglecting the small friction force acting on the test model. The coefficients of the lift and drag forces acting on the test model, C_L and C_D, were calculated based on the following expressions:

$$C_L = \frac{F_L}{\frac{1}{2}\rho U_\infty^2 D} = \frac{\frac{1}{2}\rho U_\infty^2 \sum_i C_{pi} \cdot \frac{1}{2}D\Delta\theta_i \cdot \sin\theta_i}{\frac{1}{2}\rho U_\infty^2 D}$$
$$= \frac{1}{2}\sum_i C_{pi} \cdot \Delta\theta_i \cdot \sin\theta_i$$

$$C_D = \frac{F_D}{\frac{1}{2}\rho U_\infty^2 D} = \frac{\frac{1}{2}\rho U_\infty^2 \sum_i C_{pi} \cdot \frac{1}{2}D\Delta\theta_i \cdot \cos\theta_i}{\frac{1}{2}\rho U_\infty^2 D} \quad (1)$$
$$= \frac{1}{2}\sum_i C_{pi} \cdot \Delta\theta_i \cdot \cos\theta_i$$

$$C_{pi} = \frac{p_i - p_\infty}{\frac{1}{2}\rho U_\infty^2}$$

where ρ is the air density, D is the diameter of the cylinder model, F_D and F_L are the resultant drag and lift forces acting on the cylinder models, C_{pi} is the surface pressure coefficient on the test models, p_i is the static pressure on the cylinder models, p_∞ is the static pressure of the oncoming flow, p_i and p_∞ are obtained from the DSA3217 system, θ_i is the azimuthal angle of the pressure tap, and $\Delta\theta_i$ is the angle difference between the two neighboring pressure taps. For the present study, $\Delta\theta_i = 11.25°$.

2.3 Experimental setup for PIV measurements

In addition to the surface pressure measurements with the pressure transducers, a digital PIV system was also used to conduct detailed flow field measurements to quantify the changes of the wake flow characteristics behind the test model with and without the suction flow control. In the present study, the PIV measurements were conducted in several vertical planes normal to the central axis of the test model (i.e., $X–Y$ planes as shown in Fig. 2) to reveal the changes in the shedding processes of the unsteady wake vortex structures at two sides of the test model for the cases with and without suction flow control. PIV measurements were also conducted in several horizontal planes passing or parallel to the central axis of the test model (i.e., $X–Z$ planes as shown in Fig. 2) to reveal the spanwise variations of the wake flow characteristics due to the suction flow control. For the PIV measurements, the oncoming airflow was seeded with 1–5 μm oil droplets by using a seeding generator. Illumination was provided by a double-pulsed Nd:YAG laser (New Wave Gemini PIV 200) adjusted on the second harmonic and emitting two pulses of 200 mJ at the wavelength of 532 nm with a repetition rate of 10 Hz. The laser beam was shaped to a thin sheet by a set of mirrors, spherical, and cylindrical lenses. The thickness of the laser sheet in the measurement region was about 1.0 mm. A high-resolution 12-bit (1,376 × 1,040 pixels) CCD camera (SensiCam,

Cooke Corp) was used to perform image recording for the PIV measurements. The CCD camera and double-pulsed Nd:YAG lasers were connected to a workstation (host computer) via a Digital Delay Generator (Berkeley Nucleonics, Model 565), which controlled the timing of the laser illumination and the image acquisition.

After acquiring the PIV images, instantaneous velocity vectors were obtained by frame to frame cross-correlation of the patterns of particle images, using an interrogation window of 32 × 32 pixels. An effective overlap of 50 % of the interrogation windows was employed in PIV image processing. After the instantaneous velocity vectors (u, v) were determined, instantaneous spanwise vorticity (ω_z) could be derived. The distributions of ensemble-averaged flow quantities, such as the mean velocity ($\bar{U}$, $\bar{V}$), normalized Reynolds stress ($\bar{\tau} = -\overline{u'v'}/U_\infty^2$), and turbulent kinetic energy (T.K.E. $= 0.5 \times (\overline{u'^2} + \overline{v'^2})/U_\infty^2$), were obtained from a cinema sequence of about 1,000 instantaneous PIV measurements. The measurement uncertainty level for the velocity vectors is estimated to be within 2.0 %, while the uncertainties for the measurements of ensemble-averaged flow quantities such as Reynolds stress and turbulent kinetic energy distributions about 5.0 %.

3 Measurement results and discussions

3.1 The surface pressure measurements around the test model

While Chen et al. (2013b) demonstrated that the suction flow method with isolated suction holes was very effective in suppression the VIV of a cylindrical cable model, the present work is a comprehensive experimental study to further assesses the effects of the azimuthal locations of the isolated suction holes on the effectiveness of the suction flow control. Figure 3 shows the distributions of the

Fig. 2 Schematic of the experimental setup for PIV measurements
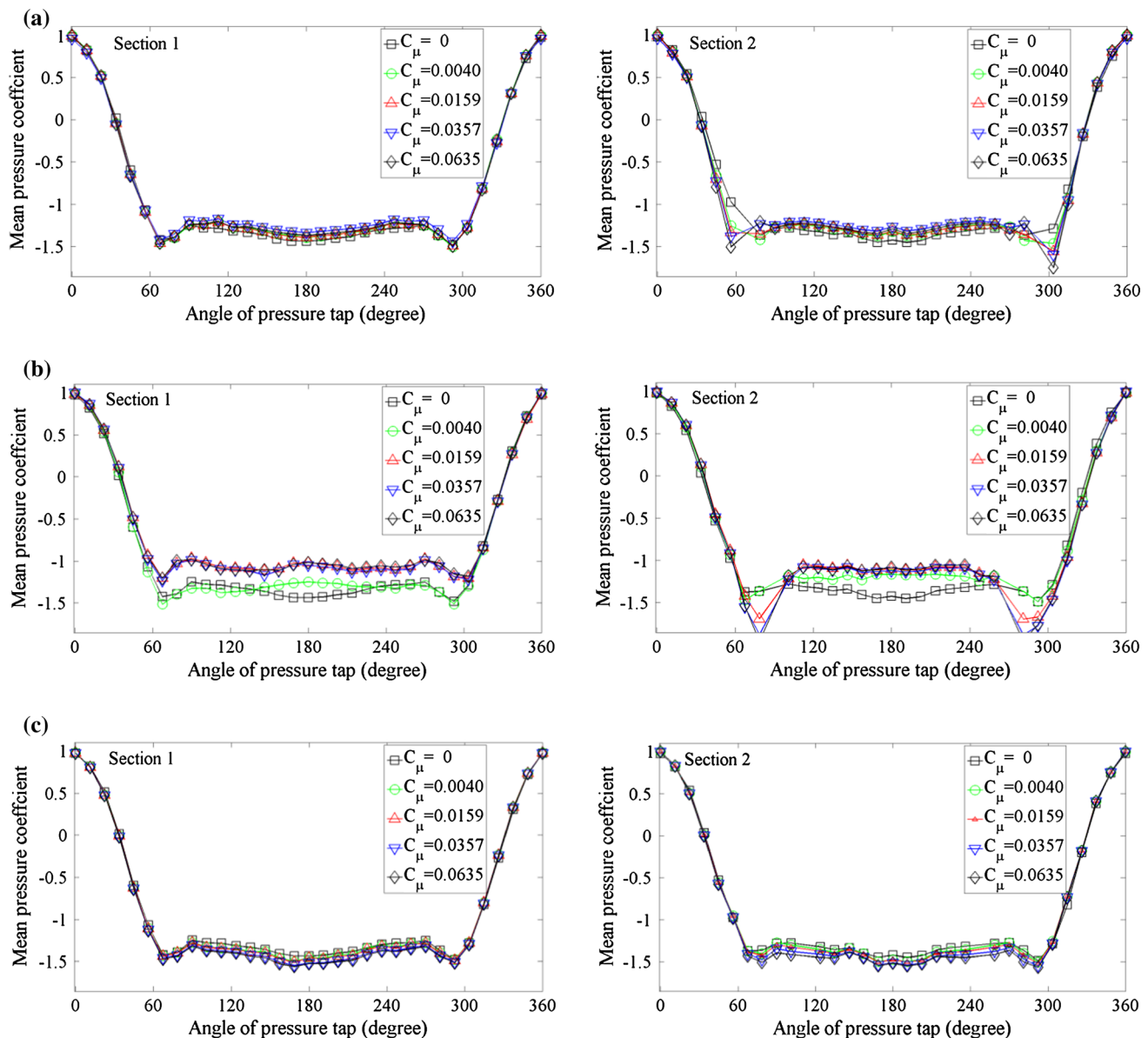
(a)

(b)

(c)
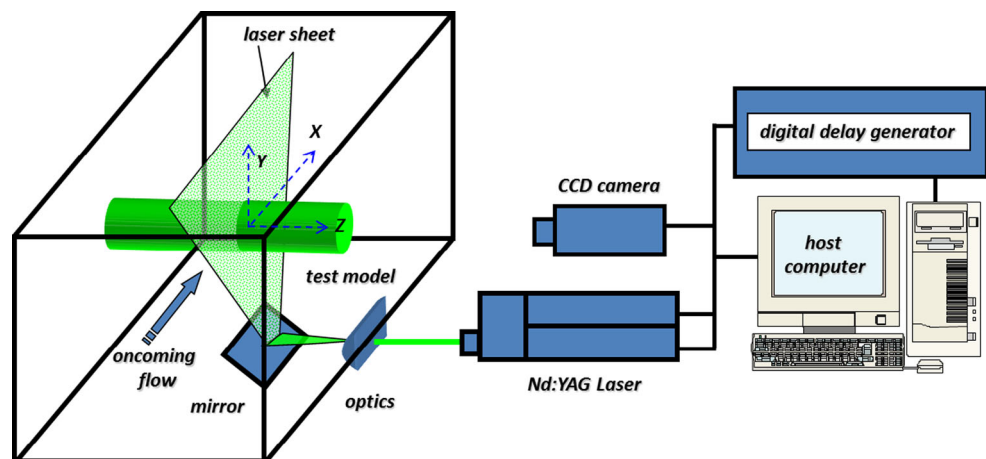
Fig. 3 Time-averaged surface pressure distributions around the test model with and without suction flow control (*left column* measurement plane #1; *right column* measurement plane #2). **a** The suction holes located at $\theta = 67.5°$ and 292.5°. **b** The suction holes located at $\theta = 90°$ and 270°. **c** The suction holes located at $\theta = 112.5°$ and 257.5°

measured mean surface pressure coefficients around the test model at measurement plane #1 (i.e., at the mid-span of the test model where no suction holes were located in the cross section) and at measurement plane #2 (i.e., the cross section with two of the pressure taps replaced by a pair of the suction holes). The spanwise spacing between the suction holes was fixed at $L_0 = L/8$. The suction flow rate through the suction holes was changed from $Q = 0$ l/min (i.e., the baseline case) to $Q = 80$ l/min, and the corresponding suction moment coefficient was in the range of $C\mu = 0 \sim 0.0635$. For the baseline case, the measurement results in Fig. 3 show that the surface pressure on the front

face of the test model (i.e., $\theta \approx 0°–67.5°$) would recover gradually and is then followed by a region with negative pressure gradients on each side of the test model (i.e., in the regions of $\theta \approx 67.5°–90°$ and $\theta \approx 270°–292.5°$). A large plateau region with an almost constant low surface pressure coefficient value was found to exist at the leeward side of the test model in the region of $\theta \approx 90°–270°$. Such a surface pressure distribution on the test model would indicate that, while the oncoming airflow was able to stay attached on the front surface of the test model, it would separate from the test model at the azimuthal locations of $\theta \approx 90°$ and 270°; namely, the separation points were

located in the neighborhood of $\theta \approx 90°$ and $270°$. It should be noted that the Reynolds number of the test cases of the present study is about 3.0×10^4, which is much less than the subcritical Reynolds number of 2.0×10^5; therefore, the flow behavior around the cylindrical test model should be subcritical, which is characterized by the existence of a laminar flow over the front surface of the circular cylinder with the flow separation points located on the windward face of the test model (i.e., $\theta \leq 90°$) (Roshko 1961; Nakamura and Tomonari 1982). A large recirculation region was found be generated in wake flow behind the test model due to flow separation. As a result, a plateau region of the surface pressure distribution was formed on the leeward surface of the circular cylinder, which is shown in Fig. 3.

As shown in Fig. 3a, when the suction holes were located at the front surface of the test model at $\theta = 67.5°$ and $292.5°$ (i.e., at the upstream locations of the separation points on the test model), the mean surface pressure distributions around the test model for the test cases with suction flow control were almost the same as those of the baseline case, regardless of the suction flow rate. Very similar trends were found for the surface pressure measurement results in both the measurement planes #1 and #2.

As shown in Fig. 3b, when the suction holes were moved to $\theta = 90°$ and $270°$ (i.e., near the separation points on the test model), the distributions of the mean surface pressure on both sides of the test model, which had negative pressure gradients and a flow separation region on the leeward side of the test model (i.e., in the region of $67.5° < \theta < 292.5°$), were found to change greatly for the test cases with the suction flow control when compared with those of the baseline case. The obvious changes in the surface pressure distributions were found in both the measurement planes #1 and #2; i.e., changes in the surface pressure distributions were found not only in the cross section with the suction holes but also in the cross section without suction holes at the mid-span of the test model. The absolute values of the negative surface pressure coefficients on the leeward surface of the test model (i.e., in the deep flow separation region) were found to initially decrease with increasing suction flow rate and then tend to flatten out when the suction flow rate exceeds $Q = 40$ l/min (i.e., $C_\mu \geq 0.0159$). It should be noted that a higher mean surface pressure on the leeward surface of the test model would indicate a smaller mean drag force acting on the test model. It can also be seen that, while the azimuthal angles of the points with the minimum mean pressure coefficient were found to always be $\theta \approx 67.5°$ and $292.5°$ at measurement plane #1 for all the test cases, the corresponding points in measurement plane #2 were further downstream at $\theta \approx 78.75°$ and $281.25°$ for the test cases with a suction flow rate greater than 40 l/min [i.e., $C_\mu \geq 0.0159$]. Consequentially, the starting points of the

plateau regions were pushed further downstream to $\theta \approx 112.50°$ and $247.50°$ in measurement plane #2. This suggests that the regions with negative pressure gradients on both sides of the test model were pushed further downstream by suction flow control; therefore, suction flow control would delay flow separation on the test model. Delayed flow separation on the test model at measurement plane #2 is visualized clearly and quantitatively in the PIV measurement results, which is discussed in the later sections of the present study.

As shown in Fig. 3c, when the suction holes were moved further downstream into the deep flow separation region on the leeward surface of the test model (i.e., at $\theta = 112.5°$ and $247.5°$), the mean surface pressure distributions on the test model under the suction flow control were nearly identical to the baseline pressure distributions. The absolute values of the negative surface pressure coefficients on the leeward surface of the test model (i.e., in the deep flow separation region) were found to become slightly greater than those of the baseline cases; therefore, suction flow control induces a slightly larger mean drag force acting on the test model.

Based on the time sequences of the measured instantaneous surface pressure distributions around the test model, the root-mean-square (RMS) values of the instantaneous pressure coefficients around the test model can be determined, which can be used to quantify the fluctuation amplitudes of the surface pressure distributions around test models, and therefore, quantify the unsteadiness of the dynamics wind loads acting on the cylindrical test model. Figure 4 shows the RMS values of the instantaneous pressure coefficients around the test model with and without suction flow control. It should be noted that a higher RMS value of the instantaneous surface pressures around on the test model would indicate a larger variation of the dynamic wind loads acting on the test model, which would cause a stronger VIV for the test model. As shown in Fig. 4, for the baseline case (i.e., the case with $C_\mu = 0$ l/min), corresponding to the shedding of the unsteady wake vortex structures from the test model, the RMS values of instantaneous surface pressures around the test model were quite high, especially in the regions near the separation points at $\theta = 90°$ and $270°$ and in the deep separation region on the leeward surface of the test model.

Figure 4a gives the measurement results with the suction holes located on the front surface of the test model (i.e., at $\theta = 67.5°$ and $292.5°$). The RMS values of the instantaneous surface pressures around the test model for the test cases with suction flow control were found to always be comparable with those of the baseline case, regardless of the suction flow rate. This indicates that suction holes located on the front surface of the test model (e.g., at $\theta = 67.5°$ and $292.5°$) perform poorly at reducing
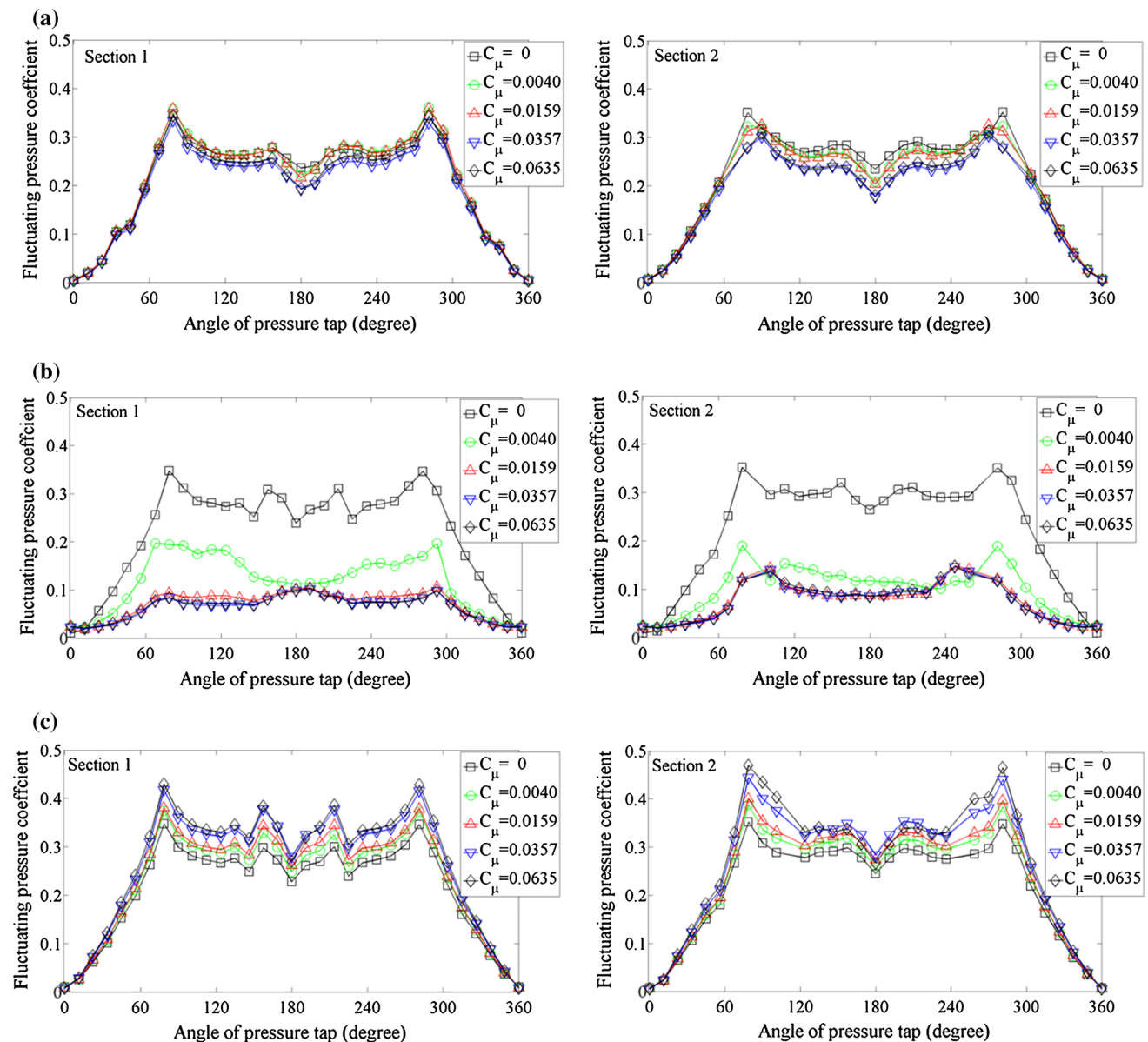
Fig. 4 The RMS values of the surface pressures around the test model with and without suction flow control (*left column* measurement plane #1; *right column* measurement plane #2). **a** The suction holes located at $\theta = 67.5°$ and $292.5°$. **b** The suction holes located at $\theta = 90°$ and $270°$. **c** The suction holes located at $\theta = 112.5°$ and $257.5°$

the amplitudes of the unsteady wind loads acting on the test model for VIV suppression.

As shown in Fig. 4b, when the suction holes were located at $\theta = 90°$ and $270°$ (i.e., near the separation points on the cylindrical test model), the RMS values of the instantaneous surface pressures around the test model were reduced significantly for the test cases with suction flow control compared to the baseline case. Even for the test case with a very small suction flow rate (i.e., $C_\mu = 0.004$), the RMS values of the instantaneous surface pressures around the test model were found to decrease to only about 50 % of those of the baseline case. As the suction flow rate

was increased to $C_\mu = 0.159$, the RMS values of the instantaneous surface pressure around the test model were found to decrease to only about 35 % of those of the baseline case. It is interesting to note that no further improvements were found in reducing the RMS values of the instantaneous surface pressure around the test model for suction flow rates $C_\mu > 0.159$. Similar results were not only found in the cross section with the suction holes, but also in the mid-span of the test model, which has a large spanwise distance of $L/16$ away from the suction holes.

Figure 4c shows the measurement results for the test cases with the suction holes moved far downstream into the

deep flow separation zone on the leeward surface the test model (i.e., at $\theta = 112.5°$ and $247.5°$). Compared with the baseline case, the RMS values of the instantaneous surface pressures around the test model for the cases with the suction flow control were found to increase gradually as the suction flow rate increased. This indicates that the unsteadiness of the dynamic wind loads acting on the test model was enhanced due to the suction flow control.

The effectiveness of the suction flow control method to reduce the unsteadiness of the dynamic wind loads acting on the test model for VIV suppression can be revealed more directly from the comparison of the time histories of the instantaneous lift and drag acting on the test model for the test cases with and without suction flow control. In the present study, the dynamic wind loads (i.e., both lift and drag forces) acting on the test model were calculated based on the measured instantaneous pressure distributions around the test model by using the Eq. (1) given above.

Figure 5 shows the time histories of the instantaneous lift coefficients of the test model for the baseline case (i.e., $C_\mu = 0.0$ case) and the cases with suction flow control at $C_\mu = 0.0040$ and $C_\mu = 0.0159$ and the corresponding power spectra obtained through a fast Fourier transform (FFT) analysis procedure, and Fig. 6 gives the time histories of the instantaneous drag coefficients for the corresponding test cases. In the plots, the gray lines denote the baseline case, and the red lines represent the test cases with suction flow control at different suction flow rates. It can be seen that, for the baseline case, the aerodynamic forces (i.e., both lift and drag forces) acting on the test model were highly unsteady with their magnitudes fluctuating significantly and randomly as a function of time. This is believed to be closely related to the shedding process of the unsteady wake vortex structures from the test model, which is revealed clearly and quantitatively from the PIV measurement results to be discussed later. It is well known that the unsteady aerodynamic forces acting on the test model excite VIV.

As shown in Figs. 5a and 6a, when the suction holes were located on the front face of the test model (i.e., $\theta = 67.5°$ and $292.5°$), the fluctuating amplitudes of the unsteady aerodynamic forces (i.e., both lift and drag forces) acting on the test model were very comparable to those of the baseline case. The corresponding power spectrum of the instantaneous lift forces reveals that the shedding frequencies of the unsteady wake vortex structures (i.e., the dominant frequency in the power spectrum) were also almost the same for the test cases with and without suction flow control. For the cases with the suction holes located at $\theta = 90°$ and $270°$ (i.e., near the separation points), the fluctuation of the dynamic aerodynamic forces (i.e., both lift and drag forces) acting on the test model was dramatically reduced, as revealed in Figs. 5b and 6b. The

shedding frequency of the unsteady wake vortex structures was also changed slightly due to the suction flow control. Furthermore, in comparison with the baseline case, not only were the fluctuation amplitudes of the instantaneous drag forces acting on the test model suppressed significantly, but the mean drag force coefficients of the test model were also found to become much smaller due to the suction flow control. This suggests that suction holes located at $\theta = 90°$ and $270°$ (i.e., near the separation points) would significantly suppress reduce the unsteadiness of the wind loads acting on the cylindrical test model for VIV suppression and greatly reduce the mean drag force acting on the test model. However, as shown in Figs. 5c and 6c, when the suction holes were moved further downstream into the deep flow separation zone on the leeward surface of the test model (i.e., at $\theta = 112.5°$ and $247.5°$), the fluctuating amplitudes of the aerodynamic forces (i.e., both lift and drag forces) acting on the test model were found to increase in comparison with the baseline case due to the suction flow control.

Based on the time sequences of the unsteady aerodynamic force measurements as those given in Figs. 5 and 6, the standard deviations of the instantaneous drag and lift forces acting on the test model can be calculated, which is used to assess the effectiveness of the suction flow control in reducing the unsteadiness of the wind loads acting on the test model for VIV suppression more quantitatively. In the present study, a non-dimensional parameter called force fluctuation reduction factor, $f_{\text{suction-control}}$, is defined as the ratio of the standard deviation values of the dynamic aerodynamic forces (either drag or lift) acting on the test model for the test case with suction flow control, $\sigma_{\text{with-control}}$, to those of the baseline case without suction flow control, $\sigma_{\text{without-control}}$; namely, $f_{\text{suction-control}} = \sigma_{\text{with-control}}/\sigma_{\text{without-control}}$ is used as a quantitative indicator to assess the effectiveness of the suction flow control under different test conditions.

It should be noted that, based on the definition given above, the force fluctuation reduction factor, $f_{\text{suction-control}}$, would have a value of 1.0 for the baseline case (i.e., the test case without suction flow control). When the value of $f_{\text{suction-control}}$ is smaller than 1.0, it indicates that the fluctuating amplitudes of the dynamic wind loads acting on the test model can be reduced by using the suction flow control method, and therefore, would offer a great potential for VIV suppression. The smaller the $f_{\text{suction-control}}$ value is, the better the performance of the suction flow control method will be for VIV suppression. However, for the test cases with the value of $f_{\text{suction-control}}$ greater than 1.0, the fluctuating amplitudes of the dynamic wind loads acting on the test model were actually enhanced by using the suction flow control method (i.e., it would promote the VIV of the test model). It should be noted that, while the test cases
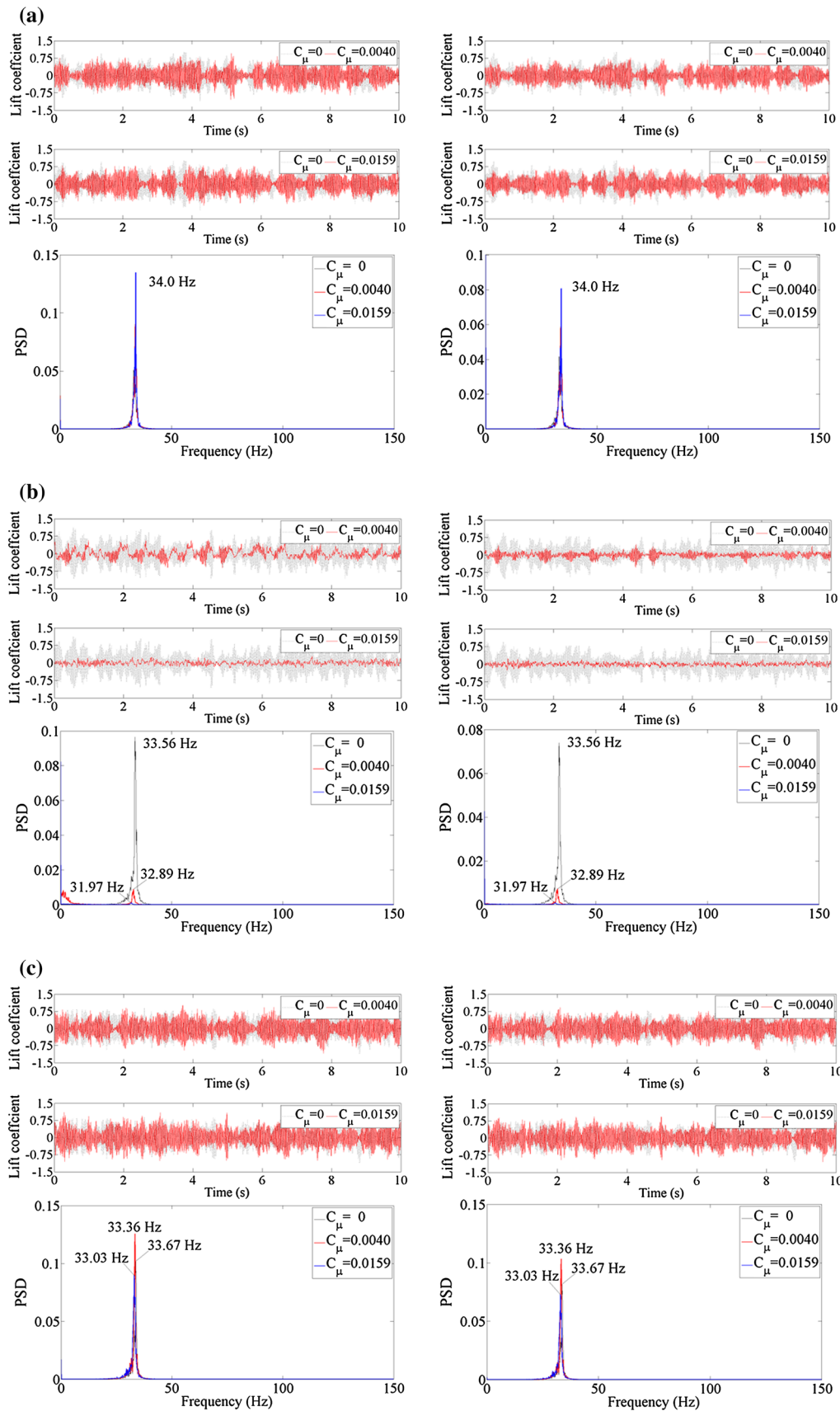
(a)

(b)

(c)

◄**Fig. 5** Time histories of the instantaneous lift coefficients and the corresponding power spectra for the test cases with and without suction flow control (*left column* measurement plane #1; *right column* measurement plane #2). **a** The suction holes located at $\theta = 67.5°$ and 292.5°. **b** The suction holes located at $\theta = 90°$ and 270°. **c** The suction holes located at $\theta = 112.5°$ and 257.5°

with $f_{\text{suction-control}}$ greater than 1.0 are not favorable for VIV suppression, these test cases would be highly desirable for the applications which rely on using vortex-induced vibration to harvest energy from the oncoming flows, such as for the vortex-induced vibration aquatic clean energy (VIVACE) converter described in Bernitsas et al. (2008).

Figure 7 gives the $f_{\text{suction-control}}$ values based on the measured lift coefficients of the test model for the test cases with and without the suction flow control. The measurement data given in Fig. 7 confirm quantitatively that the locations of the suction holes were very critical in manipulating/reducing the unsteady wind loads (i.e., aerodynamic forces) acting on the test model. When the suction holes were located at $\theta = 90°$ and 270° (i.e., near the separation points), the value of $f_{\text{suction-control}}$ was found to become dramatically smaller than 1.0. For the test case with a small suction momentum coefficient of

$C_\mu = 0.0040$, the fluctuating amplitudes of the dynamic lift forces acting on the test model were found to become only 50 and 35 % of those of the baseline case in the pressure measurement plane #1 (i.e., the cross section at the mid-span of the test model with the largest spanwise distance away from the suction holes) and the pressure measurement plane #2 (i.e., the cross section with suction holes), respectively. As the suction momentum coefficient increases to $C_\mu = 0.0159$, the fluctuating amplitudes of the lift forces acting on the test model were further decreased to only about 20 % of baseline values in both the pressure measurement plane #1 and #2. As the suction momentum coefficient exceeds $C_\mu = 0.0159$, no further significant improvements were observed. It should be noted that the values of $f_{\text{suction-control}}$ obtained from the measurement results at measurement plane #1 (i.e., the cross section at the mid-span of the test model with the largest spanwise distance away from the suction holes) were only slightly bigger than those from measurement plane #2 (i.e., the cross section with suction holes). It indicates that, even though only a limited number of isolated suction holes were used for the suction flow control, the fluctuating amplitudes of the dynamic wind loads acting on the test

Fig. 6 Time histories of the instantaneous drag coefficients with and without suction flow control (*left column* measurement plane #1; *right column* measurement plane #2). **a** The suction holes located at $\theta = 67.5°$ and 292.5°. **b** The suction holes located at $\theta = 90°$ and 270°. **c** The suction holes located at $\theta = 112.5°$ and 257.5°
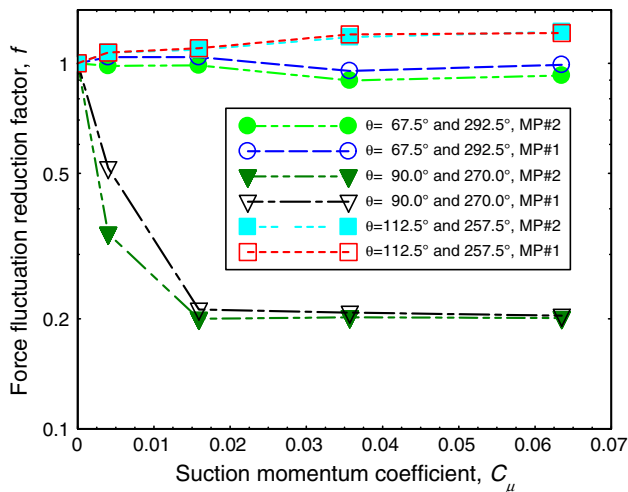
Fig. 7 The force fluctuation reduction factor versus the suction momentum coefficient
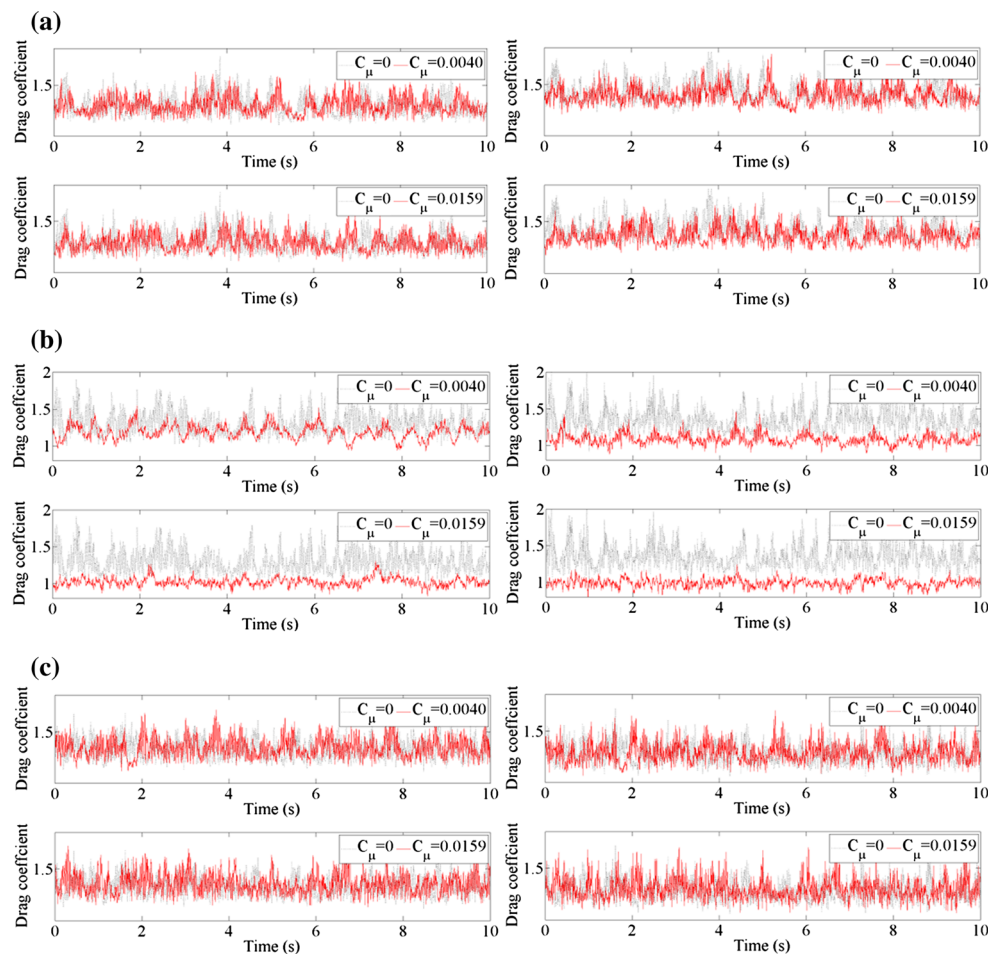
Fig. 8 The mean drag reduction factor versus the suction momentum coefficient

model can be reduced effectively, not only in the cross sections where the suction holes were located, but also along the entire span of the test model. It should be noted that, while the quantitative results given in Fig. 7 and the associated discussions given above are based on the lift measurement results, similar conclusions can also be derived from the measurement results of the drag forces acting on the test model.

It can also be seen that, for the test cases with the suction holes located on the front surface of the test model at $\theta = 67.5°$ and $292.5°$, the values of the $f_{suction-control}$ were found to always be about 1.0 (i.e., $f_{suction-control} \approx 1.0$) regardless of the suction flow rate. This indicates that suction flow control method was least effective when the suction holes are located on the windward face of the test model far away for the separation points. However, for the test cases with the suction holes located on the leeward surface of the test model (i.e., at $\theta = 112.5°$ and $247.5°$), the values of $f_{suction-control}$ were always greater than 1.0. Furthermore, the values of $f_{suction-control}$ were found to increase as the suction flow rate increased, within the range covered in the present study. This indicates that the fluctuating amplitudes of the dynamic wind loads acting on the test model were enhanced by using the suction flow control method with the suction holes moved downstream into the deep separation zone on the leeward surface the test model. This would promote, rather than suppress, the VIV of the test model.

Based on the time histories of the drag forces acting on the test model given in Fig. 6b, it can also be seen that, with the suction holes located at $\theta = 90°$ and $270°$ (i.e., near the separation points), in addition to the significant reduction in the fluctuating amplitudes of the dynamic drag forces acting on the test model, the mean drag forces acting on the test model were also found to become much smaller
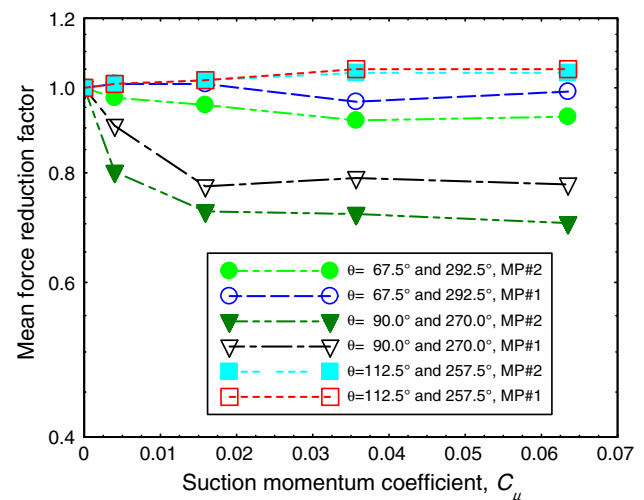
for the test cases with suction flow control when compared with the baseline case. Figure 8 shows the measured mean drag reduction factor, which is defined as the ratio of the mean drag forces acting on the test model for the test cases with the suction flow control to that of the baseline case without suction flow control (i.e., $C_{D\_with\_suction\_control}/C_{D\_without\_control}$), as a function of the suction momentum coefficient. It should be noted that, the drag coefficient for the baseline case without suction flow control was 1.24 (i.e., $C_{D\_without\_control} = 1.24$) for the present study, which agrees well with the value of $C_D = 1.20$ reported in Roshko (1961) at the Reynolds number $Re \approx 3.0 \times 10^4$.

As shown in Fig. 8, for the case with the suction holes located at $\theta = 90°$ and $270°$ (i.e., near the separation points), the mean drag coefficients of the test model were found to decrease rapidly with the increasing suction flow rate at first and then decrease gradually with a much more moderate rate for the test cases with the suction momentum coefficient $C_\mu \geq 0.0159$. For the case with the suction flow rate of $C_\mu = 0.0159$, the drag coefficient of the test model was found to decrease to about 75 % of those of the baseline case. However, within the range of the suction flow rate studied in the present study, only a very marginal reduction in the mean drag force (i.e., only a maximum drag reduction of about 5 %) can be achieved with the suction holes moved to the upwind face of the test model (i.e., at $\theta = 67.5°$ and $292.5°$). For the test cases with the suction holes moved further downstream on the leeward surface the test model (i.e., into the deep flow separation zone at $\theta = 112.5°$ and $247.5°$), the mean drag coefficients of the test models with suction flow control were always greater than the baseline value of $C_D = 1.24$ and increased gradually with the suction flow rate.

In the present study, a set of experiments were also conducted to investigate the effects of the spanwise spacing between the suction holes on the effectiveness of the suction flow control in reducing the unsteadiness of the dynamic wind loads for VIV suppression. During the experiments, the spanwise spacing (L_0) between the suction holes was doubled compared with the test cases discussed above; namely, the spanwise spacing between the suction holes was increased from $L_0 = L/8$ to $L_0 = L/4$. The general findings based on the measurement results of the test cases with the doubled spanwise spacing between the suction holes were almost the same as those described above: The azimuthal locations of the suction holes were very critical in determining the effectiveness of the suction flow control to reduce the unsteadiness of the dynamic wind loads acting on the test model for VIV suppression, and the fluctuating amplitudes of the dynamic wind loads (both lift and drag) acting on the test model can be reduced greatly when the suction holes were located at $\theta = 90°$ and $270°$ (i.e., near the separation points).

To reveal the effects of the spanwise spacing between the suction holes on the effectiveness of the suction flow control more clearly and quantitatively, Fig. 9 shows the comparison of the measurement results of the test cases with the doubled spanwise spacing between the suction holes (i.e., the test cases with $L_0 = L/4$) with those having the standard spanwise spacing (i.e., the test cases with $L_0 = L/8$) in terms of the force fluctuation reduction factor and the mean drag reduction factor with suction holes located at $\theta = 90°$ and $270°$ in respect to the oncoming airflow. It can be seen that, with the same suction flow rate or momentum coefficient, both the force fluctuation reduction factor and the mean drag reduction factor for the test cases with $L_0 = L/4$ would exceed the $L_0 = L/8$ cases. This indicates that a smaller spanwise spacing between the suction holes is favorable for the suction flow control to reduce the unsteadiness of the dynamic wind loads and the mean drag force acting on the test model.

In summary, the surface pressure measurement results given above reveal that the proper selection of the azimuthal locations for the suction holes is very critical in determining the effectiveness of the suction flow control with isolated suction holes to reduce the fluctuating amplitudes of the dynamic wind loads acting on a circular cylinder for VIV suppression. The best VIV suppression performance was achieved when the suction holes are located at $\theta = 90°$ and $270°$ (i.e., near the separation points on the test model). When the suction holes were moved upstream to the attached flow region on the front surface of the cylindrical test model, the suction flow control method was ineffective in manipulating the dynamic wind loads
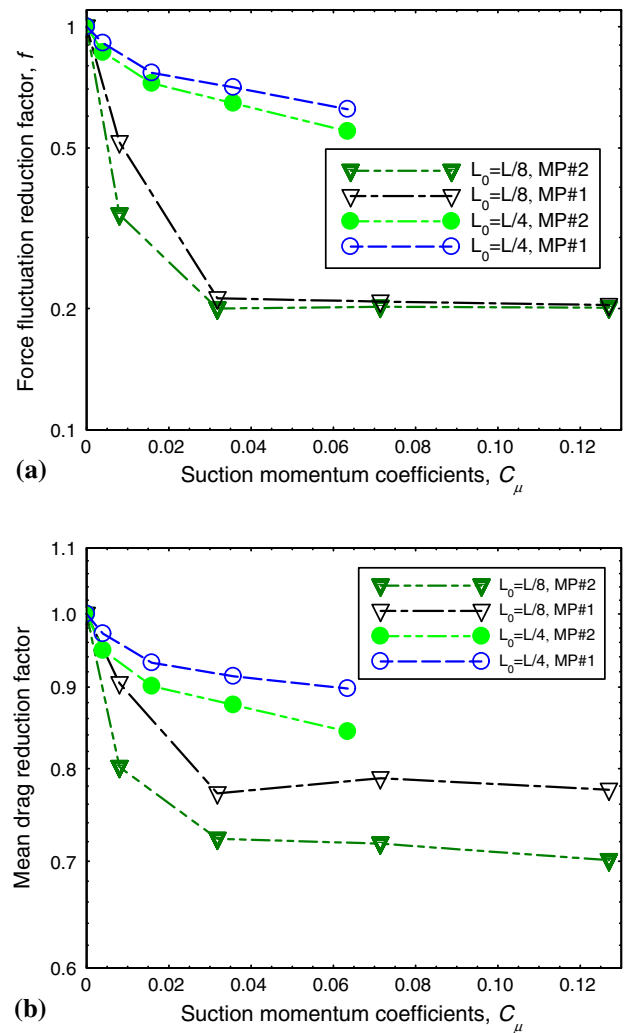

Fig. 9 Effects of the spanwise spacing between the suction holes on the effectiveness of the suction flow control. **a** Comparison of the force fluctuation reduction factor. **b** Comparison of the mean drag reduction factor

acting on the test model. When the suction holes were moved further downstream into the deep flow separation zone on the leeward surface the test model, the suction flow control method was found to actually enhance the fluctuating amplitudes of the dynamic wind loads acting on the test model, which would promote the VIV of the test model.

3.2 PIV measurement results to quantify the wake characteristics behind the test model with and without suction flow control

While the surface pressure measurement results given above reveal many interesting features and global characteristics about the suction flow control method in reducing the unsteadiness of the dynamic wind loads acting on the test
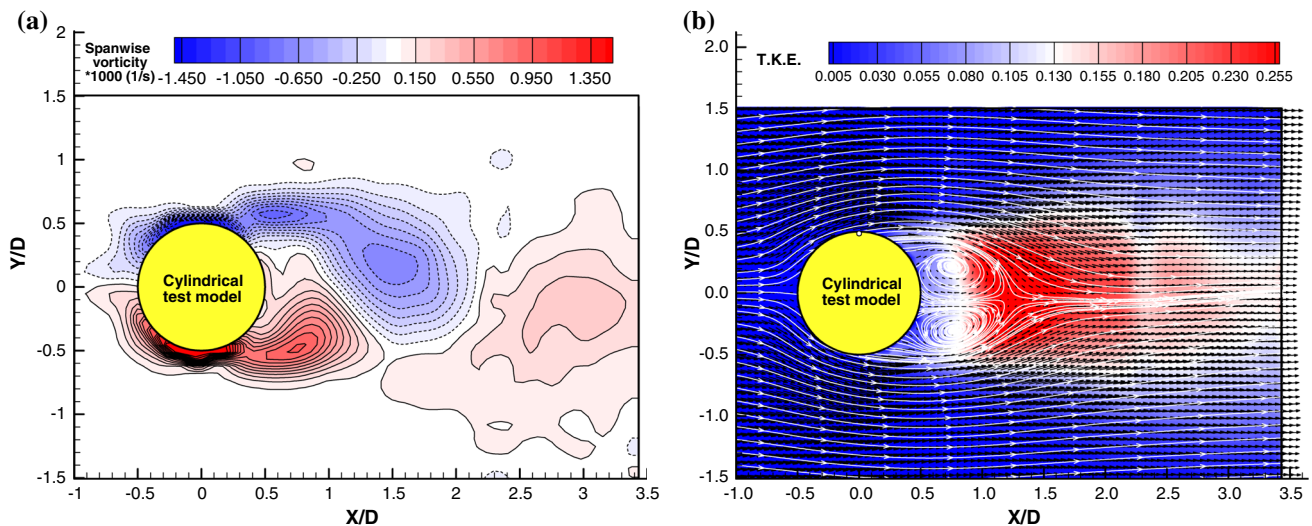
Fig. 10 The PIV measurement results for the baseline case without suction flow control. **a** Instantaneous flow field. **b** Time-averaged flow field

model, the quantitative information of the corresponding flow fields around the test model with and without suction flow control is highly desirable to gain further insight into the fundamental mechanism of the suction flow control method with isolated suction holes. A high-resolution PIV system was used in the present study to achieve detailed flow field measurements to quantify the characteristics of the wake vortex structures behind the test model.

Figure 10 shows the PIV measurement results (both instantaneous and time-averaged flow fields) of the wake flow behind the test model for the baseline case without suction flow control. As shown in the instantaneous PIV measurement, unsteady vortex structures were shed, alternating from each side of the test model to form Karman vortex streets in the wake behind the test model. The alternate shedding of the unsteady vortex structures from sides of the test model would cause dramatic variations of the surface pressures around the test model, especially in the flow separation region on the leeward side of the test model, as shown from the surface measurement results given in Fig. 4. As a result, the resultant wind loads (i.e., both lift and drag forces) acting on the test model would be fluctuating dynamically, which could excite the wind-induced vibration (VIV) of the test model. Based on the time sequences of the instantaneous aerodynamic forces acting on the test model as those shown in Figs. 5 and 6, the dominant shedding frequency of the unsteady wake vortex structures for the baseline case (i.e., without suction flow control) was $f \approx 34$ Hz. The corresponding Strouhal number was $St = fD/U_\infty = 0.21$, which was found to agree well with the measurement data reported in Kondo (1993) and Fransson et al. (2004) for the wake vortex shedding frequency from circular cylinders at the Reynolds number level of $Re \approx 3.0 \times 10^4$.

Fig. 11 PIV measurement results in the cross section with suction ▶ holes (*left* instantaneous measurement results; *right* time-averaged measurement results). **a** Suction holes located at $\theta = 67.5°$ and $292.5°$. **b** Suction holes located at $\theta = 90°$ and $270°$. **c** Suction holes located at $\theta = 112.5°$ and $247.5°$

The time-averaged PIV measurement results given in Fig. 10b reveal that the oncoming flow streams would stay attached to the windward surface of the test model at first and then separate from the surface of the test model at the azimuthal angles of $\theta \approx 90°$ and $270°$, which agrees well with the locations of the separations points identified based on the surface pressure measurement results given in Fig. 3 (i.e., the starting points of the plateau in the surface pressure profiles). As a result, a large recirculation region was found to form in the wake behind the test model. Corresponding to the alternate shedding of the unsteady vortex structures from the test model, the turbulent kinetic energy (TKE) values in the wake flow were quite high, especially along the shedding paths of the wake vortex structures. It should be noted that the TKE values in the wake flow can also be used as an indicator to assess the unsteadiness of the surface pressures around the test model and therefore the fluctuating amplitude of the resultant dynamic wind loads acting on the test model. The higher the TKE values in the wake flow are, the larger the fluctuating amplitudes of the dynamic wind loads acting on the test model will usually be.

Figure 11 gives the PIV measurement results in the cross section with suction holes (i.e., the measurement plane #2 as indicated in Fig. 1) for the test cases with the suction momentum coefficient $C_\mu = 0.0159$, and the suction holes were located at $\theta = 67.5°$ and $292.5°$, $90°$ and $270°$, $112.5°$ and $247.5°$, respectively. As shown in Fig. 11a, c, for the test cases with the suction holes moved
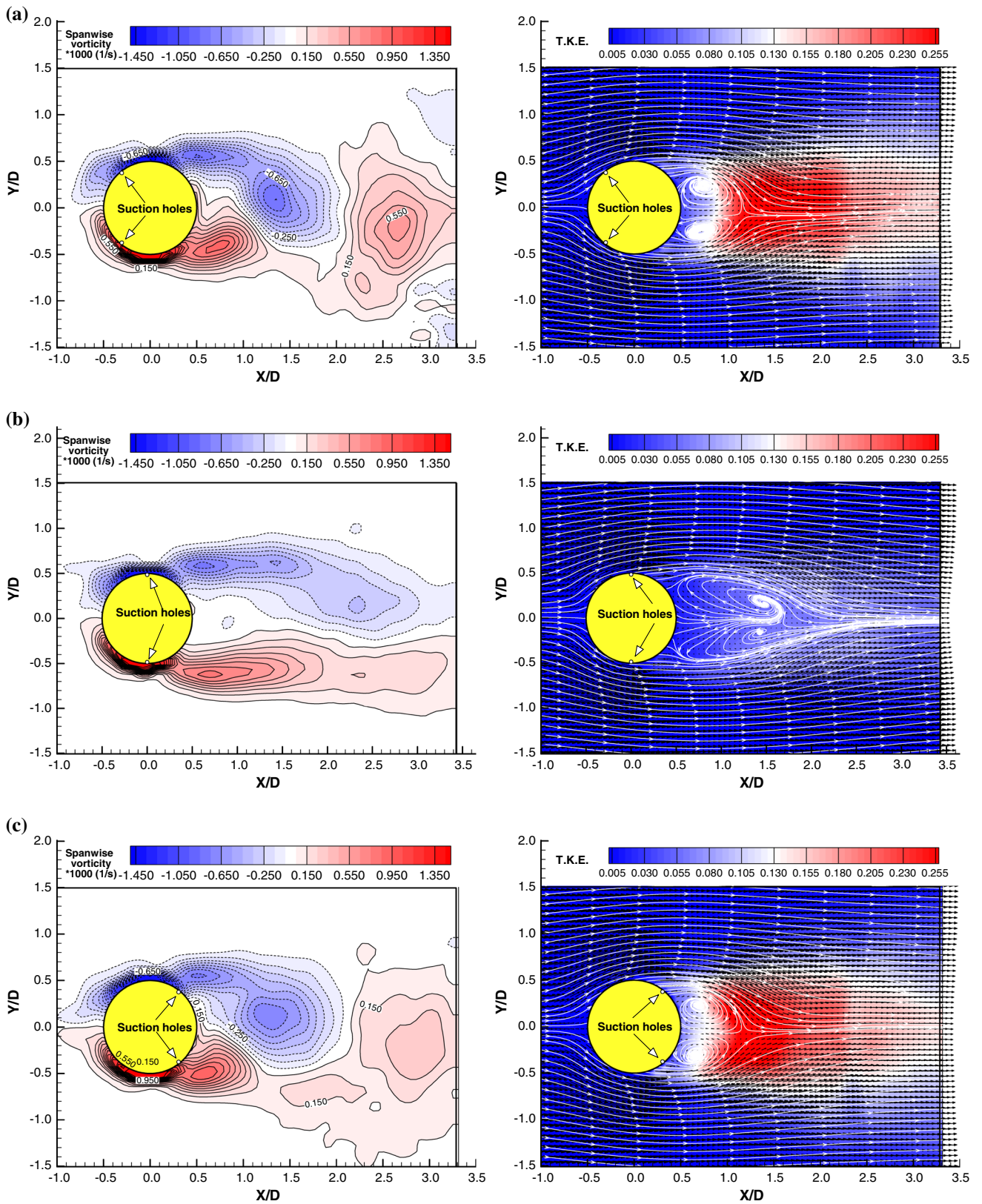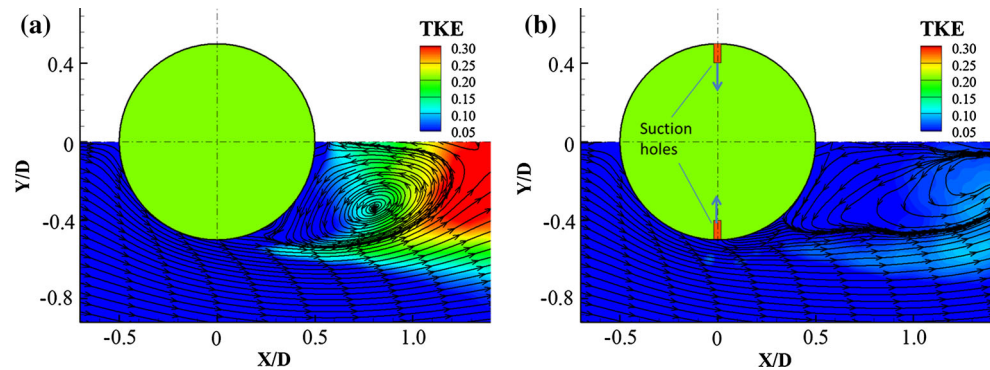
Fig. 12 The zoom-in view of the flow field near the separation points on the test model. **a** The baseline case without suction flow control. **b** With suction flow control

far away from the separation points—no matter whether the suction holes were moved upstream to the front surface side of the test model in the attached flow region (i.e., at $\theta = 67.5°$ and $292.5°$) or moved further downstream into the deep flow separation zone on the leeward surface the test model (i.e., at $\theta = 112.5°$ and $257.5°$)—the flow pattern around the test model was quite similar to those of the baseline case. On the other hand, as shown in Fig. 11b, for the case with the suction holes located near the separation points (i.e., at $\theta = 90°$ and $270°$), the instantaneous PIV measurement result reveals that the wake vortex structures at the sides of the test model were elongated significantly for the cases with the suction flow control. The alternate shedding mode of the wake vortex structures at two sides of the test model was suppressed dramatically and tended to change to a symmetric shedding mode in the near wake. It should be noted that the similar shedding mode changes of the wake vortex structures from alternate shedding mode to symmetric shedding mode were also found by Feng and Wang (2010), who used a synthetic jet located at the rear stagnation point of a circular cylinder for flow control.

As shown in Fig. 5b, the shedding frequency of the unsteady wake vortex structures was $f = 31.97$ Hz in the PIV measurement plane, which is slightly lower than that of the baseline case (i.e., $f = 33.56$ Hz). The time-averaged PIV measurement result reveals that the recirculation regions behind the test model in this PIV measurement plane were larger and longer in comparison with the baseline case. The TKE values of the wake flow were much lower since the alternate shedding of the unsteady wake vortex structures was effectively suppressed by suction flow control. The zoom-in view of the PIV results given in Fig. 12 reveals that the separation points on the test model in this PIV measurement plane (i.e., in the cross section with the suction holes) were pushed further downstream to locations up to $\theta \approx 115°$ and $245°$ due to the suction flow control, in comparison with those at $\theta \approx 90°$ and $270°$ for the baseline case. The PIV measurement results confirmed

Fig. 13 The instantaneous and time-averaged PIV measurement results in the cross sections with spanwise distances away from suction holes for the test case with the suction flow control. **a** In the cross section with a spanwise distance of 0.1 L_0 away from suction holes. **b** In the cross section with a spanwise distance of 0.3 L_0 away from suction holes. **c** In the cross section with a spanwise distance of 0.5 L_0 away from suction holes

the findings described above based on the surface pressure measurements given in Fig. 3.

As described above, with the suction holes located at $\theta = 90°$ and $270°$, significant changes in the surface pressure distributions around the test model were found not only in the cross section with the suction holes, but also in the mid-plane of the test model with the largest spanwise distance from the suction holes. In the present study, PIV measurements were also conducted in several cross sections with different spanwise distances away from the suction holes to reveal the changes of the wake flow characteristics behind the test model in the cross sections due to suction flow control, and the PIV measurement results are given in Fig. 13.

As shown in Fig. 13, the wake flow pattern behind the test model in all the studied cross sections changed greatly compared with that of the baseline case given in Fig. 10. While the recirculation region in the wake behind the test model became larger and longer as the PIV measurement plane was moved further away from the suction holes along the spanwise direction, the TKE levels in the wake flow behind the test model in all the PIV measurement planes were always much smaller than the baseline case. The PIV measurement results confirm again that the suction flow control method with isolated suction holes can manipulate/control the shedding process of the wake vortex structures effectively, not only in the cross sections with suction holes, but also in the cross sections with a spanwise distance away from the isolated suction holes. This indicates that, even though the suction holes were located on the test model as isolated point sink sources for flow control, the

(a)

(b)

(c)
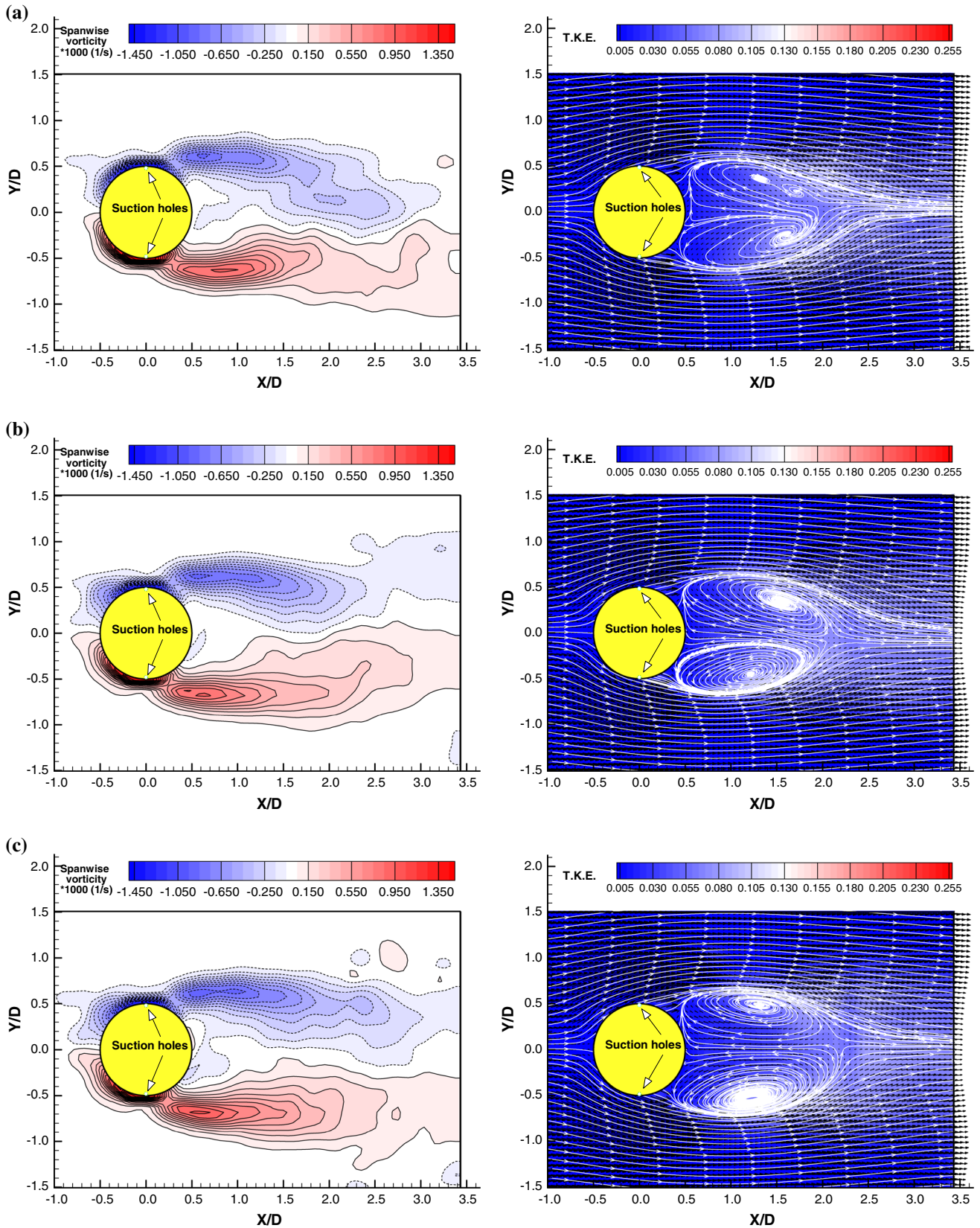
affected region of the suction flow control method can extend much further away from the suction holes along the spanwise direction in suppressing the alternate shedding of unsteady wake vortex structures from the test model, thereby, reducing the unsteadiness of the resultant dynamic aerodynamic forces acting on the test model.

To reveal more clearly the spanwise variations of the flow characteristics in the wake behind the test model due to the suction flow control, PIV measurements were also conducted in the horizontal planes (i.e., X–Z plane) parallel to the axis of the cylindrical test model. Figure 14 shows the time-averaged PIV measurement results in the horizontal plane passing through the center axis of the test model for the baseline case. Since the test model was mounted horizontally in the test section with a uniform oncoming flow, the wake behind the test model was nearly uniform along the spanwise direction; namely, the flow around the cylinder was 2-D, as expected. As shown in Fig. 14, due to the existence of the large recirculation region in the wake behind the test model, the flow velocity in the near wake next to the rear end of the test model was negative (i.e., the direction of the flow velocity is opposite to the oncoming airflow). The wake closure length of the recirculation region behind the test model (i.e., the distant between the center of the test model and the ending point of the recirculation region) was about 1.3 D for the baseline case. The flow velocity in the far wake (i.e., $X/D > 1.3$) beyond the recirculation region was in the same direction as the oncoming flow stream, as shown in Fig. 14.

Figure 15 gives the PIV measurement results of the wake flow behind the test model in four parallel horizontal planes (i.e., X–Z planes with different Y values) for the test case with the suction holes located at $\theta = 90°$ and $270°$ and the suction momentum coefficient of $C_\mu = 0.0159$. The

PIV measurement planes intersect with the test model at the azimuthal angle of $\theta = 0°$, $20°$, $42°$ and $90°$, respectively. As shown in the plots given in Fig. 15, unlike those of the baseline case having a rather uniform 2-D wake pattern behind the test model, the wake flow behind the test model with the suction flow control was much more complicated and varied significantly along the spanwise direction. As revealed from the PIV measurement result in the horizontal plane passing the center axis of the test model (i.e., in $Y = 0$ plane) given in Fig. 15a, corresponding to the four pairs of the suction holes within the PIV measurement window, four vortex structures were generated in the near wake and aligned nicely along the spanwise direction to form a rather symmetric pattern in related to the mid-span of the test model. As a result, instead of having a constant wake closure length of about 1.3 D for the baseline case, the wake closure length of the recirculation region behind the test model varied significantly along the spanwise direction for the case with the suction flow control. The wake closure length was about 2.1 D at the mid-span of the test model and decreased gradually with spanwise distance from the mid-span plane. Interestingly, the reversed flow near the rear end of the test model had almost vanished in the regions of $-1.0 < Z/D < -0.5$ and $0.5 < Z/D < 1.0$ (i.e., the regions between the suction holes at two sides of the test model), and the wake closure length in those regions was almost zero for the test case with the suction flow control. The significant spanwise variations of the wake flows and the formation of the four vortex structures behind the test model can also be seen in the other three PIV measurement planes intersecting with the test model at the azimuthal angle of $\theta = 20°$, $42°$ and $90°$ as well. It is clear that, although the suction flow control was achieved with a limited number of isolated suction holes aligned evenly along the spanwise direction of the test model, significant flow characteristics changes were induced in the wake along the entire span of the test model.

In summary, the PIV measurement results given above confirmed the findings described above based on the surface pressure measurements; namely, the azimuthal locations of the suction holes were very critical in determining the effectiveness of the suction flow control to manipulate/control the shedding process of the unsteady wake vortex structures from the test model. When the suction holes were located at $\theta \approx 90°$ and $270°$, the alternate shedding mode of the unsteady wake vortex structures was suppressed dramatically and nearly changed to a symmetric shedding mode. As a result, the fluctuating amplitudes of the resultant dynamic wind loads acting on the test model were reduced greatly due to the suction flow control method. The suction flow control method was ineffective for VIV suppression when the suction holes were moved
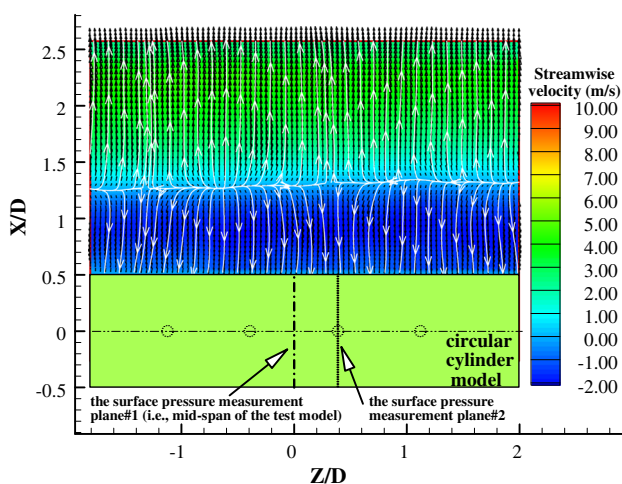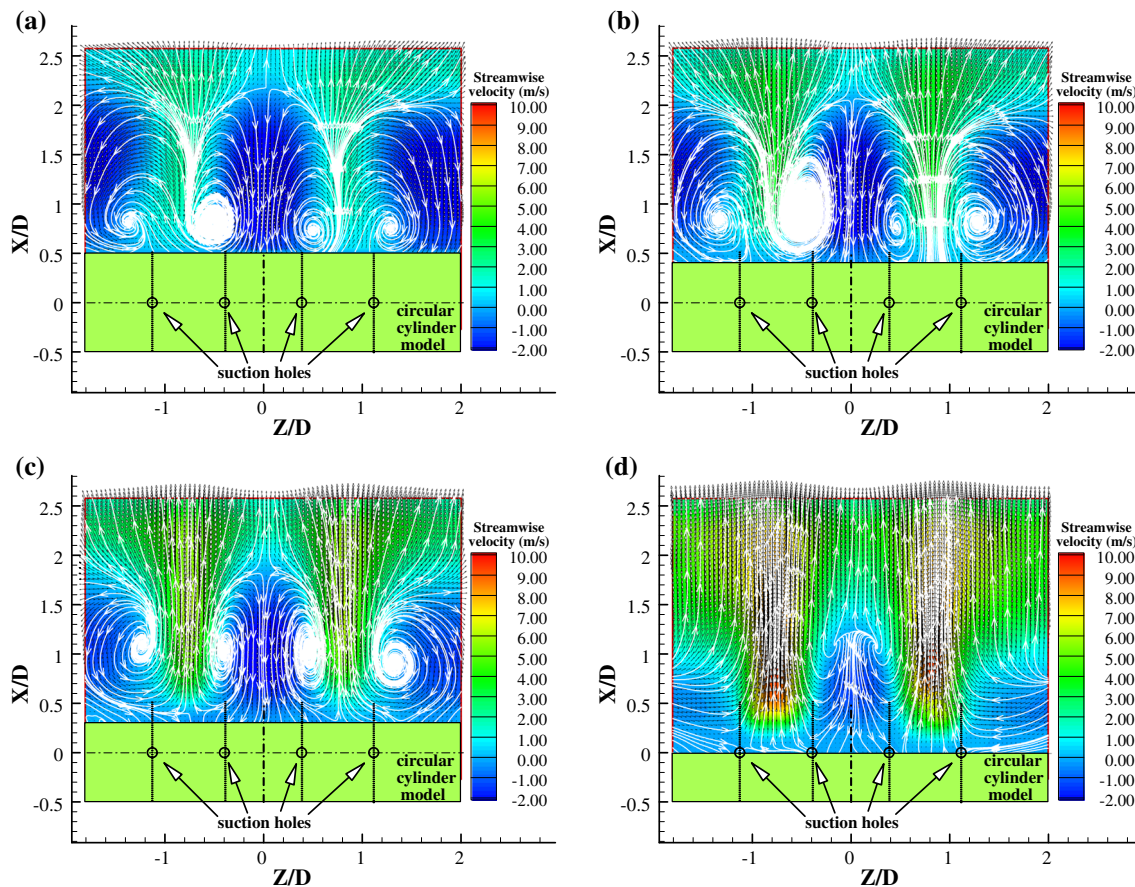

Fig. 14 Time-averaged PIV measurement result along the spanwise direction of the test model for the baseline case without suction flow control

Fig. 15 Time-averaged PIV measurement results in the horizontal planes for the test case with the suction flow control. **a** In the horizontal plane of $Y/D = 0$. **b** In the horizontal plane of $Y = D/6$. **c** In the horizontal plane of $Y = D/3$. **d** In the horizontal plane of $Y = D/2$

away from the separation points in either upstream or downstream directions.

4 Conclusions

In the present study, a comprehensive experimental study was conducted to assess the effectiveness of a suction flow control method with isolated suction holes to manipulate the vortex shedding in the wake behind a circular cylinder to reduce the fluctuating amplitudes of the dynamic wind loads acting on the cylindrical test model for VIV suppression. The azimuthal location for the suction holes is very critical in determining the effectiveness of the suction flow control to reduce the fluctuating amplitudes of the dynamic wind loads acting on the test model. When the suction holes were located at $\theta \approx 90°$ and $270°$ (i.e., near the separation points), the alternate shedding of the unsteady wake vortex structures was suppressed effectively by using the suction flow control method. As a result, the fluctuating amplitudes of the resultant dynamic wind loads acting on the test model were reduced significantly (up to

~ 80 % less), and the mean drag forces acting on the test model were reduced (up to ~ 30 % less) due to the suction flow control when compared with the baseline case. With the suction holes were moved upstream to the attached flow region on the front surface of the test model, the suction flow control method was almost invalid in manipulating the wake vortex shedding process, thereby, having almost no effects on the resultant wind loads acting on the test model. When the suction holes were moved further downstream into the deep separation zone on the leeward surface the test model, the suction flow control method actually enhanced the fluctuating amplitudes of the dynamic wind loads acting on the test model, which would promote the VIV of the test model.

Although the suction flow control method used in the present study was achieved with a limited number of isolated suction holes aligned evenly along the spanwise direction of the cylindrical model, the shedding process of the wake vortex structures behind the test model changed significantly over the entire span of the test model. This indicates that the region affected by suction flow control is not limited to the cross sections with the suction holes, but

also includes cross sections with substantial spanwise distance from the suction holes. While the baseline exhibited a spanwise-invariant wake, the wakes behind the suction flow controlled test models were much more complicated and varied significantly in the spanwise direction. As a result, the wake closure length also varied significantly along the spanwise direction of the test model for the cases with the suction flow control. In these cases, the wake closure length in the regions between the suction holes nearly decreased to zero; consequently, the reversed flow region in the near wake nearly vanished.

References

Barlow JB, Rae WH, Pope A (1999) Low-speed wind tunnel testing, 3rd edn. Wiley, New York, pp 330–375

Bernitsas MM, Raghavan K, Ben-Simon Y, Garcia EMH (2008) VIVACE (vortex induced vibration aquatic clean energy): a new concept in generation of clean and renewable energy from fluid flow. ASME J Offshore Mech Arct Eng Trans 130(4):041101-15

Chen WL, Li H, Ou JP, Li FC (2011) Field monitoring of vortex induced vibration of stay cables of cable-stayed bridge. In: 9th International symposium on cable dynamics, Shanghai, China, pp 257–264

Chen WL, Tang SR, Li H, Hu H (2013a) Influence of dynamic properties and position of rivulet on rain-wind-induced vibration of stay cables. ASCE J Bridge Eng 18(10):1021–1031

Chen WL, Xin DB, Xu F, Li H, Ou JP, Hu H (2013b) Suppression of vortex-induced vibration of a circular cylinder using suction-based flow control. J Fluids Struct 42(10):25–39

Chng TL, Rachman A, Tsai HM, Zha GC (2009) Flow control of an airfoil via injection and suction. J Aircraft 46(1):291–300

Feng LH, Wang JJ (2010) Circular cylinder wake vortex synchronization control with synthetic jet positioned at back stagnation point. J Fluid Mech 662:232–259

Feng LH, Wang JJ (2012) Synthetic jet control of separation in the flow over a circular cylinder. Exp Fluids 53:467–480

Feng LH, Wang JJ, Pan C (2010) Effect of novel synthetic jet on wake vortex shedding modes of a circular cylinder. J Fluids Struct 26:900–917

Feng LH, Wang JJ, Pan C (2011) Proper orthogonal decomposition analysis of vortex dynamics of a circular cylinder under synthetic jet control. Phys of Fluid 23:014106-1–014106-13

Fransson JHM, Alfredsson PH (2003) On the disturbance growth in an asymptotic suction boundary layer. J Fluid Mech 482:51–90

Fransson JHM, Konieczny P, Alfredsson PH (2004) Flow around a porous cylinder subject to continuous suction or blowing. J Fluids Struct 19:1031–1048

Gbadebo SA, Cumpsty NA, Hynes TP (2008) Control of three-dimensional separations in axial compressors by tailored boundary layer suction. J Turbomach 130(011004):1–8

Glezer A, Amitay M (2002) Synthetic jets. Annu Rev Fluid Mech 34:503–529

Grager T, Rothmayer A, Hu H (2011) Stall suppression of a low-Reynolds-number airfoil with a dynamic burst control plate. In: 49th AIAA aerospace sciences meeting including the new horizons forum and aerospace exposition, AIAA 2011–1180, Orlando, FL

Greenblatt D, Paschal KB, Yao CS, Harris J, Schaeffler NW, Washburn AE (2006) Experimental investigation of separation control Part 1: baseline and steady suction. AIAA J 44(12):2820–2830

Hikami Y, Shiraishi N (1988) Rain-wind induced vibrations of cables in cable stayed bridges. J Wind Eng Ind Aerodyn 29:409–418

Irwin HPAH, Cooper KR, Girard R (1979) Correction of distortion effects caused by tubing systems in measurements of fluctuating pressures. J Wind Eng Ind Aerodyn 5:93–107

Kondo N (1993) Direct third-order upwind finite element simulation of high Reynolds number flows around a circular cylinder. J Wind Eng Ind Aerodyn 46:349–356

Li H, Chen WL, Xu F, Li FC, Ou JP (2010) A numerical and experimental hybrid approach for the investigation of aerodynamic forces on stay cables suffering from rain–wind induced vibration. J Fluid Struct 26(7–8):1195–1215

Main JA, Jones NP (1999) Full-scale measurements of stay cable vibration. In: 10th International conference on wind engineering (10ICWE). Wind Engineering into the 21st century, 1–3, pp 963–970

Matsumoto M, Shirato H, Yagi T, Goto M, Sakai S, Ohya J (2003) Field observation of the full-scale wind-induced cable vibration. J Wind Eng Ind Aerodyn 91:13–26

Modi VJ (1997) Moving surface boundary-layer control: a review. J Fluids Struct 11:627–663

Munshi SR, Modi VJ, Yokomizo T (1997) Aerodynamics and dynamics of rectangular prisms with momentum injection. J Fluids Struct 11:873–892

Nakamura Y, Tomonari Y (1982) The effects of surface roughness on the flow past circular cylinders at high reynolds numbers. J Fluid Mech 123:363–378

Owen JC, Bearman PW (2001) Passive control of VIV with drag reduction. J Fluids Struct 15:597–605

Patil SKR, Ng TT (2010) Control of separation using spanwise periodic porosity. AIAA J 48(1):174–187

Patnaik BSV, Wei GW (2002) Controlling wake turbulence. Phys Rev Lett 88:35–40

Qin N, Zhu Y, Poll DIA (1998) Surface suction on aerofoil aerodynamic characteristics at transonic speeds. Proc Inst Mech Eng Part G J Aerosp Eng 212(5):339–351

Roshko A (1955) On the wake and drag of bluff bodies. J Aeronaut Sci 22:124–132

Roshko A (1961) Experiments on the flow past a circular cylinder at very high Reynolds number. J Fluid Mech 10:345–356

Seal CV, Smith CR (1999) The control of turbulent end-wall boundary layers using surface suction. Exp Fluids 27:484–496

Wu CJ, Wang L, Wu JZ (2007) Suppression of the von Karman vortex street behind a circular cylinder by a traveling wave generated by a flexible surface. J Fluid Mech 574:365–391

Zuo D, Jones NP (2010) Interpretation of field observations of wind- and rain-wind-induced stay cable vibrations. J Wind Eng Ind Aerodyn 98:73–87

Zuo D, Jones NP, Main JA (2008) Field observation of vortex- and rain-wind-induced stay-cable vibrations in a three-dimensional environment. J Wind Eng Ind Aerodyn 96:1124–1133